ChemComm

COMMUNICATION

View Article Online
View Journal | View Issue

Cite this: *Chem. Commun.*, 2026, **62**, 8235

Received 6th February 2026,
Accepted 24th March 2026

DOI: 10.1039/d6cc00813e

rsc.li/chemcomm

Imine linkers enable the formation of robust single-molecule junctions

Yidong Xiao,†[a] Chaochao Xie,†[b] Ya-Qi Kong,[c] Guang-Ping Zhang,*[c] Xuefeng Tan*[b] and Haixing Li*[a]

While imine (C═N) groups are renowned for their role in dynamic chemistry, whether imine binds to Au electrodes for forming single-molecule junctions and their electronic properties remain elusive. We demonstrate that imine groups serve as chemical anchors for the reliable formation of single-molecule junctions with gold electrodes and imine-terminated wires show slightly higher conductance than their amine-terminated analogues. Critically, stable junction formation under steric hindrance is achieved with imines when amines fail. These results establish imines as versatile linkers for molecular junction design.

In the field of single-molecule electronics, the scanning tunneling microscope-based break junction (STM-BJ)[1–3] has emerged as a cornerstone technique for probing charge transport through single-molecule circuits, enabling the efficient repeated creation of molecular junctions. The stability and electronic properties of molecular junctions critically depend on the anchoring groups (linkers) that bridge molecules and electrodes, the design of which directly governs device performance. The exploration of novel linkers remains a vital focus in molecular electronics.

In recent years, imine (C═N) groups have garnered significant attention in materials science owing to their unique chemical properties.[4,5] Imine bonds not only exhibit dynamic reversibility, enabling tunable formation and cleavage under pH or redox stimuli,[6,7] but also their conjugated structures enhance electronic delocalization across molecular frameworks, thereby improving the charge transport efficiency. For instance, in covalent organic frameworks, imine linkages have facilitated exceptional photocatalytic and charge-separation performance through π–π stacking and conjugation effects.[8–10] Moreover, the inherent dynamic nature of imines has unlocked opportunities in molecular machines and stimuli-responsive materials, such as light- or electric field-driven conformational switching.[11–13] These attributes suggest that imines may serve as promising linkers in single-molecule electronics, combining stability with functional tunability. Specifically, a recent work by Zhang *et al.* demonstrates that photo-generated iminyl radicals enable the creation of highly conductive molecular junctions through formation of covalent N–Au bonds on gold surfaces.[14] Nevertheless, systematic investigations into imines as molecular anchors remain scarce, and their chemical/physical interactions with electrodes, as well as their conductance characteristics, are yet to be elucidated.

Herein, we report an investigation of imine linkers in single-molecule junctions by break-junction measurements and density functional theory (DFT) calculations. Through comparative analyses of junction formation and conductance characteristics between imine- and amine-linked systems, this work unravels the unique advantages of imines in forming dative N→Au bonds as the steric blockage of nearby phenyl groups does not inhibit the binding. DFT calculations corroborate our experimental observation that in comparison with the C–N bond, C═N conjugation on a gold-bound nitrogen slightly enhances the junction conductance.

We design compounds **1** and **2**, which comprise one (**1**) or two (**2**) benzene(s) terminated with a C-phenyl imine, where the phenyl is attached to the carbon atom on the imine (chemical structure in Fig. 1c and d) and a thiomethyl group on the other end. Attempts to obtain a pure terphenyl compound were unsuccessful due to the poor solubility of the terphenyl moiety, which made purification difficult. A thiomethyl linker is installed for forming dative bonds between the molecule and Au surfaces.[15] Compounds **1** and **2** were readily prepared by reacting benzonitrile with corresponding aryl Grignard reagents (see the SI).[16] We performed the single-molecule conductance measurements of 1 mM target molecule **1** or **2** in 1,2,4-trichlorobenzene (TCB) at 0.9 V tip bias using the scanning tunneling microscope-based break junction (STM-BJ) technique at room temperature under ambient conditions.

[a] *Department of Physics, City University of Hong Kong, Kowloon 999077, Hong Kong SAR, China. E-mail: haixinli@cityu.edu.hk*
[b] *Department of Chemistry, City University of Hong Kong, Kowloon 999077, Hong Kong SAR, China. E-mail: xuefetan@cityu.edu.hk*
[c] *School of Physics and Electronics, Shandong Normal University, Jinan 250358, China. E-mail: zhangguangping@sdnu.edu.cn*
† These authors contributed equally to this work.

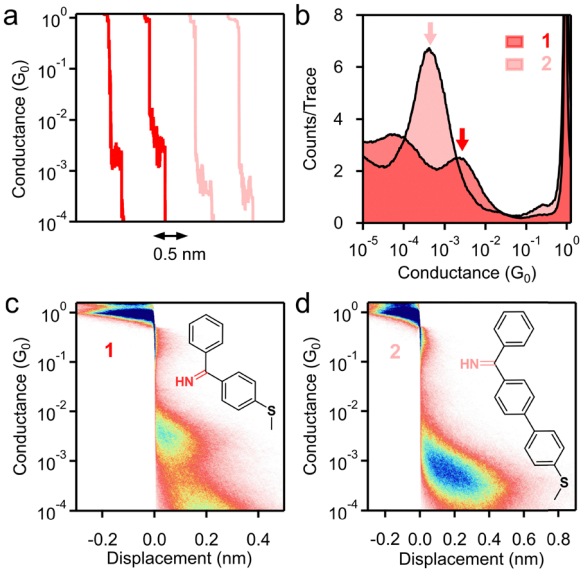

Fig. 1 (a) Representative individual traces from a single-molecule conductance measurement of **1** and **2** in TCB. (b) 1D conductance histograms of **1** and **2** measured at 0.9 V. (c) and (d) 2D conductance histograms of (c) **1** and (d) **2** measured at 0.9 V.

In individual conductance traces measured for **1** and **2**, we observed well-defined molecular plateaus, signifying stable molecular junction formation, as shown in Fig. 1a.

As shown in Fig. 1b, we observe distinct conductance peaks for **1** and **2** (indicated by arrows) that arise from single-molecule junctions formed between **1**/**2** and Au electrodes. Gaussian fits yield peak conductance values of $2.1 \times 10^{-3}G_0$ ($G_0 = 2e^2/h$) and $4.2 \times 10^{-4}G_0$ for **1** and **2**, respectively, consistent with the length-dependent exponential decay characteristic of the electron coherent transport process. For comparison, we also performed STM-BJ measurements on 4-(methylthio)aniline (structure in Fig. S1), which resembles the structure of **1** but does not contain the sp^3 carbon; we expect to see an enhanced charge transport in 4-(methylthio)-aniline in comparison with **1**. Indeed, 4-(methylthio)aniline exhibits a single-molecule junction conductance of $\sim 10^{-2}G_0$ (Fig. S1 and Table S1). The corresponding junction elongation lengths of **1** and **2** derived from 2D histograms (Fig. 1c and d) are ~0.26 nm and ~0.55 nm, respectively. We note that a broad low conductance peak is seen for **1** and we hypothesize that it is a signature for π–π stacked dimer junctions, as suggested by previous single-molecule conductance studies.[17–22]

A junction similar to that of **2**, except for that a covalent N–Au bond was formed by imine radicals, was reported to show a single-molecule conductance of 1.6×10^{-3} G_0,[14] which is larger than the conductance of **2** by a factor of 3.8. This conductance increase (3.8×) for a junction with one linkage changing from a dative N→Au to a covalent N–Au bond seems rather modest considering a factor of 20 was seen for a few other compounds undergoing the similar transition from dative N→Au to covalent N–Au bonds for one linkage (400× increase if it occurs for both linkages).[23] We emphasize two differences between these two cases. First, the factor 3.8 is observed for imine linkers and the factor 20 was observed for primary amine linkers; the C═N in imines and C–N in amines could lead to different electronic transport properties. Second, the factor 3.8 is observed for two junctions that also differ by one phenyl group attached at the imine carbon position (this phenyl group in **2** is not present in the compound Al-2 reported by Zhang *et al.*), and this structural change has an impact on the junction geometry, which could also affect the conductance. It comes to our attention that the same N–Au covalently linked imine junction as that shown in ref. 14 was reported to exhibit a lower conductance in a separate work (summarized in Table S1, Al-1 junction *versus* ZL-05 junction).[24] Since ZL-05 in ref. 24 under UV shows a conductance similar to that of **1** (0.7×) in our work, we propose the possibility in ref. 24 that imines were formed from imine radicals upon hydrogen abstraction from solvent or adventitious water in the environment, which subsequently bind to Au electrodes *via* dative bonds.

We further measured the conductance of **1** and **2** at 90 mV and 450 mV and found robust junction formation by the imine linker at both low and high bias voltages with almost the same single-molecule conductance (Fig. S2 and S3). Next, we evaluated the single-molecule conductance of compounds **1** and **2** in a polar propylene carbonate (PC) solvent. A wax-coated tip was used for reducing the background ionic current that stems from the use of the polar solvent.[25] As shown in Fig. S4 and S5, the imine linker maintains excellent junction formation in a polar environment, and the conductance values for **1** and **2** are nearly identical to those measured in a non-polar TCB solvent. These results collectively demonstrate that imine, as a linker group, can form stable single-molecule junctions under different applied voltages and solvent environments.

As imine is demonstrated to form a robust linkage with Au electrodes, we next evaluate its electronic properties by comparing *C*-phenyl imine with *N*-phenyl imine and other amine anchoring motifs. The chemical structures of **3**–**5** are depicted in Fig. 2a, where we see that all share the same benzene backbone and thiomethyl linker group. **3** bears a primary amine (–NH_2) terminus and lacks the benzene ring connected to the carbon present in **1**. Crucially, **4** serves as the direct structural analog to **1** as they are identical in backbone architecture and anchor groups, differing solely in the C═NH → C–NH_2 conversion (Fig. 2a). If the presence of the phenyl ring in **1** adds steric hindrance for the access of lone pair of electrons on the nitrogen by Au electrodes, then compound **4** provides a direct comparison with **1**. In comparison with **1**, compound **5** features phenyl substitution on the imine nitrogen (Ph–N═C) rather than on the carbon (N═C–Ph), with a methyl group at the imine carbon position. Amine **4** was obtained by reducing compound **1** with $NaBH_4$.[16] Imine **5** was prepared by reacting 4-thiomethyl acetophenone with aniline under dehydration conditions (see the SI).[26]

We measured the single-molecule conductance of **3**, **4**, and **5** by using a 1 mM solution of the target molecule in TCB at 0.9 V and present the 1D histograms in Fig. 2b. Similar to **1**, compound **3** exhibits a primary conductance peak at $1.7 \times 10^{-3}G_0$

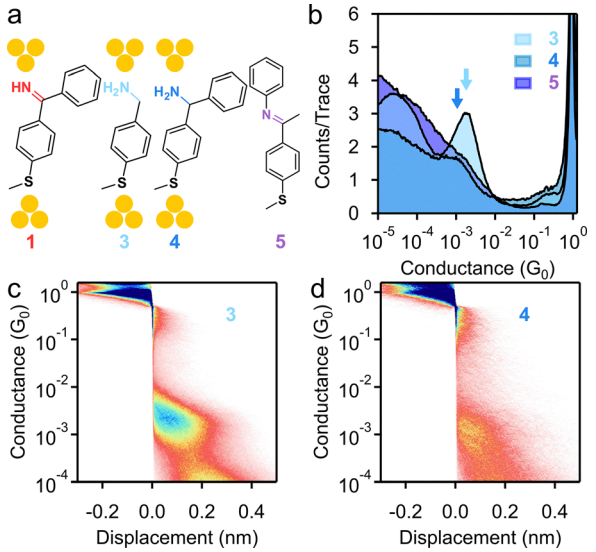

Fig. 2 (a) Chemical structures of **1**, **3**, **4**, and **5**. (b) 1D conductance histograms of **3**, **4**, and **5** measured at 0.9 V. (c) and (d) 2D conductance histograms of (c) **3** and (d) **4** measured at 0.9 V.

corresponding to the single-molecule junction conductance with a junction elongation length of ~0.31 nm (Fig. 2c). The comparable conductance values of **1** and **3** suggest that imine provides an electronic transport pathway that is as efficient as the most commonly used primary amine linker. We next focus on **4**, which does not display a well-defined conductance peak. **4** shows a peak-like feature of low-intensity at around $1 \times 10^{-3} G_0$ with an elongation length of ~0.29 nm (Fig. 2d and S6). We suggest that this suppressed junction formation originates from a weakened binding between the amine and Au atoms due to steric hindrance by the adjacent phenyl ring at the nitrogen. The robust binding of **1** and weak binding of **4** to Au electrodes highlight the unique different binding characteristics between imines and amines when used as linker groups.

It is noteworthy that compound **5** does not show any conductance peaks. It has been reported before that compared to the primary amine (R-NH_2) linker, secondary amines (R-$NHCH_3$) show suppressed binding in regular STM-BJ experiments due to the steric hindrance produced by the methyl group.[3,27] This observation is also consistent with earlier studies reporting that the compounds containing *N*-phenyl imines were connected to the electrodes by other linker groups, suggesting no binding between *N*-phenyl substituted imines and Au electrodes.[28,29] We thus suggest that for **5**, the steric hindrance caused by the phenyl group prevents the contact formation between the imine nitrogen and the gold electrode.

As imine is shown to form robust contact with Au electrodes when a thiomethyl group is installed as the linker for the other end, we next determine, when no thiomethyl group is present, whether a dual-anchored double-imine architecture can form single-molecule junctions. We design compound **6** (chemical structure is given in Fig. 3a), which can be readily synthesized using a similar method to the synthesis of **1** and **2**, but with 1,4-dicyanobenzene as the starting material (see the SI).[30] The 1D

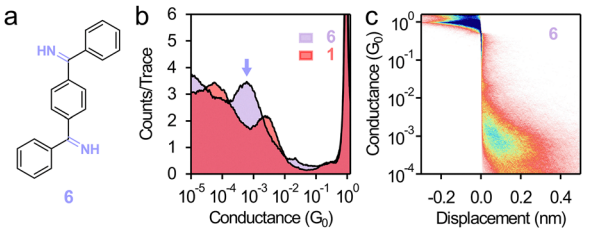

Fig. 3 (a) Chemical structure of **6**. (b) 1D and (c) 2D conductance histograms of **6** measured at 0.9 V. Data of **1** are reproduced in (b) for comparison.

and 2D conductance histograms of **6** (Fig. 3b and c) exhibit a well-defined peak at $5.5 \times 10^{-4} G_0$ with a junction elongation length of 0.37 nm, confirming that a molecule terminated with two imine linker groups on the two ends forms stable single-molecule junctions. We find that the conductance of 1,4-bis(methylthio)benzene (**7**, chemical structure in Table S1, two thiomethyl linkers) is 4.7 times higher than that of **1** (one thiomethyl and one imine),[14] and the conductance of **1** is 3.8 times higher than that of **6** (two imines). This comparison illustrates that substituting one linker and substituting the second linker both lead to a 4 times conductance change.

A relevant conductance comparison is between **6** and 1,4-bis((methylthio)methyl)benzene (**8**, $3.3 \times 10^{-4} G_0$, chemical structure in Table S1),[31] as they share a similar backbone structure, junction length, and dative interactions with Au electrodes. We find that the conductance of **6** is ~1.7-fold higher than that of **8**, underscoring the enhanced electronic coupling afforded by the imine–Au interaction. We observe the same single-molecule conductance value for **6** under 90 mV and 450 mV bias voltages (Fig. S7) as well as in polar solvent PC (Fig. S8). These findings further demonstrate that imine forms stable contact with Au electrodes in non-polar and polar environments. Altogether, these results (summarized in Table S1) show that the imine motif offers a new approach to link organic species to Au electrodes.

Density functional theory (DFT) calculations are further conducted to evaluate the conductance properties of imines and amines within the QuantumATK package.[32–34] A detailed analysis of the conformational differences between imines and amines at the N–C1–C2–C3 dihedral angle (Fig. 4a) is provided in Fig. S9. When we optimize junction structures after the gold electrodes are attached to the molecule, we see that the junction of **4** shows a large steric hindrance from the phenyl ring, which is absent in junctions of **1** and **3** (Fig. 4b). We thus hypothesize that the suppressed junction formation for **4** in comparison with **1** seen in the experiments is possibly arising from the steric hindrance of the phenyl ring, which hinders the interaction or effective binding of the amine group with the Au electrode. To assess the relative stability of the junctions, we calculate the binding energies between the Au surface and **1**, **3**, and **4** (Table 1). At their most stable configurations, **1** exhibits the strongest binding to the Au electrode (−0.99 eV), followed by **3** (−0.88 eV) and **4** (−0.79 eV). This trend is consistent with the experimental observations, where **1** shows a higher junction formation probability compared to that of **4**, suggesting that the reduced junction formation of **4** is

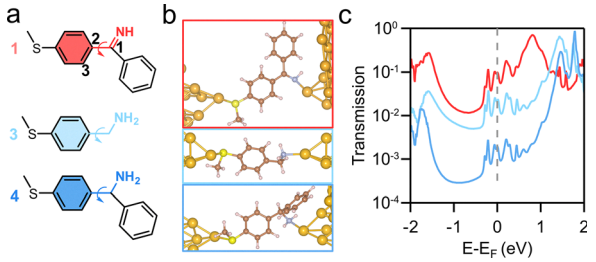

Fig. 4 (a) Schematic of the N–C1–C2–C3 dihedral angle ω studied for compounds **1**, **3**, and **4**. Colored arrows indicate the direction of rotation for an increasing ω. (b) Optimized structures of single-molecule junctions of **1**, **3**, and **4**. (c) Calculated transmissions for junctions of **1**, **3**, and **4**.

Table 1 Calculated binding energies (eV) between nitrogen in **1**, **3**, and **4** and Au electrodes at different N–C1–C2–C3 dihedral angles (ω)

Molecule	ω (°)	Binding energy (eV)	Molecule	ω (°)	Binding energy (eV)
1	159	**−0.99**	**3**	149	−0.85
	199	−0.91		329	**−0.88**
	339	−0.94	**4**	29	−0.55
	379	−0.62		209	**−0.79**

associated with a weaker nitrogen–Au interaction due to the steric hindrance of the phenyl ring.

We further calculated the transmissions for compounds **1**, **3**, and **4** within the QuantumATK package.[32–35] As shown in Fig. 4c, the transmission coefficients at the Fermi level (E_F) (reflecting the conductance of the junctions at low bias voltages) follow the order T (**1**) > T (**3**) > T (**4**), in agreement with the conductance trend seen in the break-junction experiments. The increased conjugation in **1** seems to be captured by the transmission, as we find that in comparison with **3** and **4**, **1** exhibits a smaller gap between the highest occupied molecular orbital (HOMO) and the lowest unoccupied molecular orbital (LUMO). Overall, we demonstrate that the imine-terminated molecule confers a slightly higher conductance than its amine analog.

In this study, we investigate the potential of imine (C═N) groups as novel anchoring linkers in single-molecule electronics. Through synthesis, STM-BJ experiments, and DFT calculations, we demonstrate that imine can form stable and conductive molecular junctions. Crucially, in comparison with primary amines, imines demonstrate comparable and even slightly enhanced electronic transport efficiency and superior binding in cases where steric hindrance is present. The single-molecule conductance peak observed in dual-imine systems further underscores their robustness as linkers. These results position imines as versatile linkers at the interface between organic compounds and Au surfaces. We envisage that this imine–Au anchoring strategy will expand the molecular toolbox for constructing adaptive nanoelectronics.

Conflicts of interest

There are no conflicts to declare.

Data availability

The data supporting this study are available within the article and its supplementary information (SI). Supplementary information is available. See DOI: https://doi.org/10.1039/d6cc00813e.

Additional data are available from the corresponding author upon reasonable request.

Acknowledgements

H. L. acknowledges the support from the Research Grants Council of the Hong Kong SAR, China (project no. 21310722 and 11304723), the Natural Science Foundation of Guangdong Province, China (project no. 2025A1515011929), and the City University of Hong Kong through a start-up fund. X. T. acknowledges the support from the Research Grants Council of the Hong Kong SAR, China (project no. 21304324). G. Z. acknowledges the support from the National Natural Science Foundation of China (Grant No. 22173052).

References

1 B. Q. Xu and N. J. J. Tao, *Science*, 2003, **301**, 1221–1223.
2 L. Venkataraman, J. E. Klare, C. Nuckolls, M. S. Hybertsen and M. L. Steigerwald, *Nature*, 2006, **442**, 904–907.
3 L. Venkataraman, J. E. Klare, I. W. Tam, C. Nuckolls, M. S. Hybertsen and M. L. Steigerwald, *Nano Lett.*, 2006, **6**, 458–462.
4 K. Yamamoto, M. Higuchi, S. Shiki, M. Tsuruta and H. Chiba, *Nature*, 2002, **415**, 509–511.
5 W. G. Xu and N. Yoshikai, *Angew. Chem., Int. Ed.*, 2016, **55**, 12731–12735.
6 L. Q. Li, X. T. Peng, D. Zhu, J. Zhang and P. Xiao, *Macromol. Chem. Phys.*, 2023, 224.
7 M. Kathan, C. Jurissek, P. Kovarícek and S. Hecht, *J. Polym. Sci., Part A: Polym. Chem.*, 2019, **57**, 2378–2382.
8 T. T. Feng, D. Streater, B. Sun, K. Duisenova, D. Wang, Y. Liu, J. E. Huang and J. Zhang, *J. Phys. Chem. Lett.*, 2022, **13**, 1398–1405.
9 D. H. Streater, E. R. Kennehan, D. A. Wang, C. Fiankor, L. J. Chen, C. Q. Yang, B. Li, D. H. Liu, F. Ibrahim, I. Hermans, K. L. Kohlstedt, L. Luo, J. Zhang and J. R. Huang, *J. Am. Chem. Soc.*, 2024, **146**, 4489–4499.
10 H. He, R. C. Shen, Y. H. Yan, D. J. Chen, Z. X. Liu, L. Hao, X. Zhang, P. Zhang and X. Li, *Chem. Sci.*, 2024, **15**, 20002–20012.
11 L. Greb and J. M. Lehn, *J. Am. Chem. Soc.*, 2014, **136**, 13114–13117.
12 Y. X. Deng, Q. Zhang and B. L. Feringa, *Adv. Sci.*, 2024, **11**, 2308666.
13 J. R. Wu, L. Kreimendahl and J. L. Greenfield, *Angew. Chem., Int. Ed.*, 2025, **64**, e202415464.
14 M. L. Zhang, J. F. Lin, K. Song, K. L. Chang, X. J. Dai, Y. P. Zang and D. B. Zhu, *J. Am. Chem. Soc.*, 2023, **145**, 6480–6485.
15 Y. S. Park, A. C. Whalley, M. Kamenetska, M. L. Steigerwald, M. S. Hybertsen, C. Nuckolls and L. Venkataraman, *J. Am. Chem. Soc.*, 2007, **129**, 15768- +.
16 K. Zhang, X. F. Liu, W. Z. Zhang, W. M. Ren and X. B. Lu, *Org. Lett.*, 2022, **24**, 3565–3569.
17 K. Homma, S. Kaneko, K. Tsukagoshi and T. Nishino, *J. Am. Chem. Soc.*, 2023, **145**, 15788–15795.
18 R. Frisenda, V. Janssen, F. C. Grozema, H. S. J. van der Zant and N. Renaud, *Nat. Chem.*, 2016, **8**, 1099–1104.
19 A. Magyarkuti, O. Adak, A. Halbritter and L. Venkataraman, *Nanoscale*, 2018, **10**, 3362–3368.
20 Y. X. Tang, Y. Zhou, D. H. Zhou, Y. R. Chen, Z. Y. Xiao, J. Shi, J. Y. Liu and W. J. Hong, *J. Am. Chem. Soc.*, 2020, **142**, 19101–19109.
21 X. H. Li, Y. Zheng, Y. Zhou, Z. Y. Zhu, J. Y. Wu, W. H. Ge, Y. X. Zhang, Y. Q. Ye, L. C. Chen, J. Shi, J. Y. Liu, J. Bai, Z. T. Liu and W. J. Hong, *J. Am. Chem. Soc.*, 2023, **145**, 21679–21686.
22 Y. Q. Zhang, Y. X. Zhang, L. Wang, C. Zhang and H. L. Chen, *Trends Chem.*, 2025, **7**, 299–316.

23 Y. P. Zang, A. Pinkard, Z. F. Liu, J. B. Neaton, M. L. Steigerwald, X. Roy and L. Venkataraman, *J. Am. Chem. Soc.*, 2017, **139**, 14845–14848.
24 T. Zhang, T. W. Li, J. S. Li, Z. F. Yu, H. Chen, M. J. Li, J. X. Yu, S. J. Zhen and Z. J. Zhao, *Chem. Eng. J.*, 2025, **520**, 165691.
25 L. A. Nagahara, T. Thundat and S. M. Lindsay, *Rev. Sci. Instrum.*, 1989, **60**, 3128–3130.
26 Z. H. Li, L. Zhang, M. Nishiura and Z. M. Hou, *ACS Catal.*, 2019, **9**, 4388–4393.
27 W. Y. Guo, T. Quainoo, Z. F. Liu and H. X. Li, *Chem. Commun.*, 2024, **60**, 3393–3396.
28 S. H. Choi, B. Kim and C. D. Frisbie, *Science*, 2008, **320**, 1482–1486.
29 Z. L. Miao, T. Quainoo, T. M. Czyszczon-Burton, N. Rotthowe, J. M. Parr, Z. F. Liu and M. S. Inkpen, *Nano Lett.*, 2022, **22**, 8331–8338.
30 Z. Gomurashvili and A. S. Hay, *J. Macromol. Sci., Part A: Pure Appl. Chem.*, 2005, **A42**, 127–138.
31 H. Vazquez, R. Skouta, S. Schneebeli, M. Kamenetska, R. Breslow, L. Venkataraman and M. S. Hybertsen, *Nat. Nanotechnol.*, 2012, **7**, 663–667.
32 S. Smidstrup, T. Markussen, P. Vancraeyveld, J. Wellendorff, J. Schneider, T. Gunst, B. Verstichel, D. Stradi, P. A. Khomyakov, U. G. Vej-Hansen, M.-E. Lee, S. T. Chill, F. Rasmussen, G. Penazzi, F. Corsetti, A. Ojanperä, K. Jensen, M. L. N. Palsgaard, U. Martinez, A. Blom, M. Brandbyge and K. Stokbro, *J. Phys.: Condens. Matter*, 2020, **32**, 015901.
33 QuantumATK version P-2019.03, Synopsys QuantumATK (https://www.synopsys.com/manufacturing/quantumatk.html) (accessed August 20, 2025).
34 M. Brandbyge, J.-L. Mozos, P. Ordejón, J. Taylor and K. Stokbro, *Phys. Rev. B: Condens. Matter Mater. Phys.*, 2002, **65**, 165401.
35 D. Stradi, U. Martinez, A. Blom, M. Brandbyge and K. Stokbro, *Phys. Rev. B*, 2016, **93**, 155302.